Hindawi
Mathematical Problems in Engineering
Volume 2020, Article ID 8709870, 13 pages
https://doi.org/10.1155/2020/8709870

Research Article

Dynamics Parametrization and Calibration of Flexible-Joint Collaborative Industrial Robot Manipulators

Emil Madsen,[1,2] **Simon Aagaard Timm**,[1,2] **Norbert Andras Ujfalusi**,[1,2] **Oluf Skov Rosenlund**,[1] **David Brandt**,[1] **and Xuping Zhang**[2]

[1]*Universal Robots A/S, Energivej 25, Odense S DK-5260, Denmark*
[2]*Aarhus University, Inge Lehmanns Gade 10, Aarhus C DK-8000, Denmark*

Correspondence should be addressed to Emil Madsen; emil_madsen@hotmail.com and Xuping Zhang; xuzh@eng.au.dk

Received 1 May 2020; Revised 18 July 2020; Accepted 24 July 2020; Published 17 September 2020

Academic Editor: Jürgen Pannek

Many collaborative robots use strain-wave-type transmissions due to their desirable characteristics of high torque capacity and low weight. However, their inherent complex and nonlinear behavior introduces significant errors and uncertainties in the robot dynamics calibration, resulting in decreased performance for motion and force control tasks and lead-through programming applications. This paper presents a new method for calibrating the dynamic model of collaborative robots. The method combines the known inverse dynamics identification model with the weighted least squares (IDIM-WLS) method for rigid robot dynamics with complex nonlinear expressions for the rotor-side dynamics to obtain increased calibration accuracy by reducing the modeling errors. The method relies on two angular position measurements per robot joint, one at each side of the strain-wave transmission, to effectively compensate the rotor inertial torques and nonlinear dynamic friction that were identified in our previous works. The calibrated dynamic model is cross-validated and its accuracy is compared to a model with parameters obtained from a CAD model. Relative improvements are in the range of 16.5% to 28.5% depending on the trajectory.

1. Introduction

For collaborative industrial robots, it is of crucial importance to acquire accurate predictions of the torques required in order to realize the desired motion or force control task and to ensure a consistently good performance of lead-through programming applications. Being able to accurately predict the torques required to complete the intended task will (1) improve the control performance by being able to react to disturbances before they cause deviations from the reference and (2) improve the robot safety system by being able to more accurately identify external disturbances such as human interference. Accurate torque estimates can be obtained through knowledge about the dynamic properties of the robot. Accurate torque estimates will also improve any possible online estimation procedures such as online estimation of the payload mass and inertia properties [1], friction, and/or wear.

The dynamic model of the robot relates the robot motion to the joint torques and it depends on a set of dynamic parameters being the mass, the first moments, and the mass moments of inertia of each link of the robot. Multiple procedures exist for estimating the dynamic parameters of robot manipulators:

(1) *Physical Experiments.* The robot is disassembled to isolate each link. The mass can be evaluated directly. The first moments can be obtained by evaluating the counterbalanced points of each link. The diagonal elements of the inertia tensor can be evaluated by pendular motions. Such methods are tedious and are not preferred because they require a lot of manual operations to disassemble the robot and carry out the experiments. Furthermore, experiments need to be redone if hardware changes are made to the robot.

(2) *Computer Aided Design (CAD).* The dynamic parameters of each link are found using their nominal

geometric and material characteristics. In the design phase, such investigation can be used in the performance analysis to further improve the design. However, the accuracy of the parameter estimates is reduced because the CAD parts are never identical to the real parts due to the production tolerances.

(3) *System Identification*. The input/output behavior is analyzed on some planned motion. Parameters are estimated by minimizing the difference between the measured output (possibly the current supplied to the electric actuator) and its mathematical model evaluated in the input (possibly the angular positions of the robot joints). Such procedures are preferred because they generally lead to the most accurate results while offering flexibility in the case of robot hardware changes.

For system identification methods, the most common strategy is a combined Inverse Dynamics Identification Model and Least Squares (IDIM-LS) method. For such method, the accuracy of the parameter estimates is generally affected by measurement noise and modeling errors.

The issue of measurement noise is often addressed by generating so-called exciting trajectories and/or filtering the noisy measurements [2]. Other identification techniques have also been suggested such as the Extended Kalman Filter (EKF) [3, 4], algorithms based on Linear Matrix Inequality (LMI) tools [5], maximum likelihood (ML) approaches [6], the Set Membership Uncertainty [7], and Huber's estimator [8]. However, based on the experimental results, these approaches do not improve the IDIM-LS, and they were not validated on 6-degrees-of-freedom (DOF) industrial robots. To eliminate the need for tuning the bandpass filters that are applied to the trajectory data, [9, 10] used the Instrumental Variable (IV) technique, and [11] proposed the Direct and Inverse Dynamic Identification Models (DIDIM) technique. These methods are based on a closed-loop output error (CLOE) method using both the direct and inverse dynamic models of the robot. The direct dynamic model is used to obtain model-based estimates of the position, velocity, and acceleration signals in contrast to the bandpass filtering often coupled with the IDIM-LS method. In [12], the DIDIM and CLOE methods were compared to the IDIM-LS method and it was found that if the IDIM-LS method is coupled with well-tuned bandpass filtering, the DIDIM and CLOE methods do not offer any improvements to the IDIM-LS method. Other methods include identifying the dynamics of a robotics system using neural networks [13].

Modeling errors will generally lead to a bias of the parameter estimates and it is an issue yet unsolved in the system identification for industrial robots. Modeling errors arises mainly from neglecting the complex and nonlinear joint dynamics effects resulting in significant deterministic structural errors that cannot be accounted for by random variables. Such nonlinear joint dynamics come, for instance, due to the use of strain-wave type transmissions such as the Harmonic Drive™ which are often used in collaborative robots due to their desirable characteristics of high torque capacity and low weight.

The works on the identification of dynamic parameters for collaborative robots are limited. In [14], the essential parameters were identified for the KUKA LWR 4+ collaborative robot assuming a three-parameter friction model. In [1, 15], dynamics parameter identification was performed using the KUKA LWR 4+ collaborative robot with friction neglected. The works on the KUKA LWR 4+ collaborative robot exploited the joint torque sensor located on the output side of the transmission; thus the joint dynamics do not affect the measurements. Such sensor hardware is, however, expensive and is rarely found in industrial robots. In [16], the dynamic parameters for the 7 DOF Franka Emika Panda robot were identified with a constrained optimization procedure to ensure the physical consistency of the parameters. In [17], the parameters for the 2×7 DOF ABB IRB 14000 (YuMi) collaborative robot were identified. The fact that very simple models of the friction are employed with Coulomb and linear viscous friction and that joints are assumed rigid are common in the mentioned works. Such assumptions on the joint dynamics characteristics for strain-wave transmissions are serious simplifications of the real dynamic characteristics.

To address the mentioned limitations of the prior art, we propose a new method for estimating the dynamic parameters of collaborative robot manipulators considering the flexible joint dynamics effects. Firstly, the dynamics of the Universal Robots UR5e collaborative robot manipulator are developed in closed form using the modified Denavit-Hartenberg convention and the Recursive Newton–Euler Algorithm. Secondly, the dynamic equations are linearly parametrized and the dimension of the parameter space is reduced to a minimum. Thirdly, the proposed rotor dynamics compensation is introduced to reduce modeling errors. The novelty lies in the rotor dynamics compensation in which *two* built-in rotary encoders are utilized per joint, one at each side of the transmission element, to effectively compensate the complex nonlinear joint dynamics effects of the Universal Robots UR5e robot manipulator identified prior to this work [18,19]. Any unmodeled friction is handled by augmenting the set of dynamic parameters with Coulomb and viscous friction coefficients for each joint. The parameters are then estimated by a WLS procedure with the weighting equal to the inverse of the estimated covariance matrix. Lastly, the calibrated dynamic model is validated on new trajectories that were not used for the estimation (cross-validation principle). The general methodology of the dynamics calibration in this work is illustrated in Figure 1. The two-encoder setup is illustrated by the *Robot* outputting two angular position variables q and θ for the link and rotor, respectively.

The distinguished contributions of this work include the following: (1) a linear parametrization describing the dynamics of the UR5e collaborative robot manipulator has been developed, (2) the complex nonlinear dynamic friction characteristics and rotor inertia have been considered, (3) the minimal set of base parameters that describe the dynamic behavior of the UR5e robot has been accurately estimated, and (4) the performance of the calibrated dynamic model has been validated.

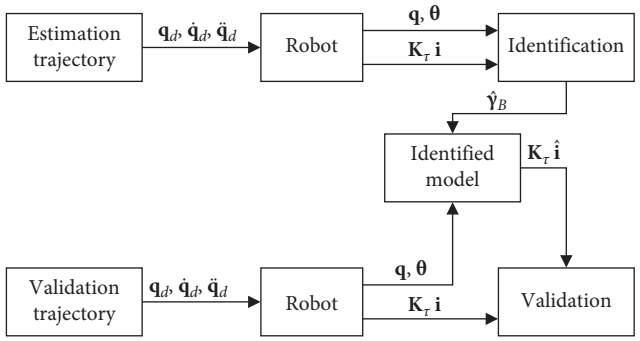

Figure 1: Schematic representation of the methodology of this work showing the interconnection between the identification and validation procedures.

The rest of the paper is organized as follows: Section 2 describes the mathematical model of the Flexible-Joint Robot (FJR) manipulator. In Section 3, the linear parametrization of the dynamics is described. In Section 4, the identification procedure is described and the results of the identification are presented. In Section 5, the calibrated dynamic model is validated and compared to a model obtained with parameters from a CAD model. Section 6 concludes the work and presents the challenges for our ongoing research.

1.1. Notations. The notation used in the paper is mostly standard. Let $\mathbb{R}$ be the set of real numbers, $\mathbb{N}$ be the set of nonnegative integers, and $\mathbb{N}^+$ be the set of positive integers. Let $\mathbf{x} \in \mathbb{R}^n$ be a vector of n real numbers; then x_i is its i^{th} entry, $\mathbf{x}^T$ its transpose, $\overline{\mathbf{x}}$ is the mean value of the elements of $\mathbf{x}$, and $\|\mathbf{x}\|$ is the 2-norm. Let $\widehat{\mathbf{x}}$ denote an estimate of $\mathbf{x}$ and let $\widetilde{\mathbf{x}} \triangleq \mathbf{x} - \widehat{\mathbf{x}}$ be the estimation error. Given a function g: $\mathcal{G} \longrightarrow \mathbb{R}$, let sgn: $\mathbb{R} \longrightarrow \{-1, 0, 1\}$ be the signum function defined such that $\text{sgn}(g) = -1$ if $g < 0$, $\text{sgn}(g) = 0$ if $g = 0$, and $\text{sgn}(g) = 1$ if $g > 0$. If $\mathbf{g}$: $\mathcal{G} \longrightarrow \mathbb{R}^n$ is a vector function, the signum vector function $\mathbf{sgn}(\mathbf{g}) = [\mathbf{sgn}(\mathbf{g}_1) \cdots \mathbf{sgn}(\mathbf{g}_n)]^T$. Given a square real matrix $\mathbf{A} \in \mathbb{R}^{n \times n}$, let $\mathbf{A} > 0$ indicate that $\mathbf{A}$ is positive definite; that is, $\mathbf{x}^T \mathbf{A}\, \mathbf{x} > 0$ for any nonzero column vector $\mathbf{x}$ of n real numbers. Let diag: $\mathbb{R}^n \longrightarrow \mathbb{R}^{n \times n}$ map a vector of n elements to a diagonal matrix with the i^{th} element of the vector on its i^{th} diagonal entry and zero everywhere else. Similarly, let diag^{-1}: $\mathbb{R}^{n \times n} \longrightarrow \mathbb{R}^n$ map the diagonal elements of an $n \times n$ matrix to vector of n elements with the i^{th} diagonal element of the matrix on the i^{th} element of the vector.

2. Mathematical Model

The Flexible-Joint Robot (FJR) manipulator is considered as an open kinematic chain having $N + 1$ rigid bodies; the base and the N links are interconnected by N revolute joints undergoing deflection and actuated by N electrical actuators. To derive the dynamics of the robot manipulator, the following standard assumptions are made:

(i) The rotors are uniform bodies having their center of mass on the axis of rotation

(ii) Each motor $i = 1, \ldots, N$ is mounted on link $i - 1$ and moves link i; see Figure 2

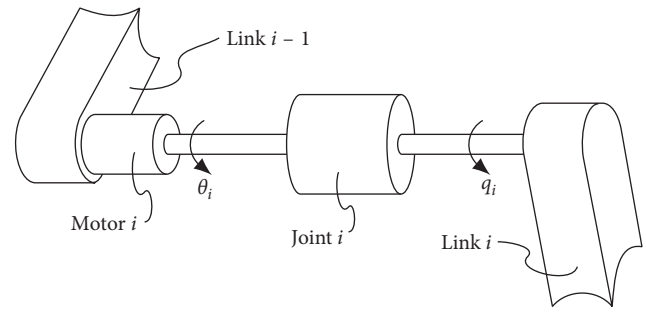

Figure 2: Kinematic arrangement of motors and links for the FJR manipulator model. Note that θ_i is already scaled by the reduction ratio.

Assumption (i) is a basic requirement for long life of an electrical drive and implies that the robot dynamics become independent of the angular position of the rotors. For the UR5e manipulator, we take advantage of the presence of large reduction ratios and simply assume the following.

(iii) The angular velocity of the rotors is due only to their own spinning

This simplifying assumption was proposed by [20] and is equivalent to neglecting energy contributions due to the inertial couplings between the rotors and the links. It also implies that Coriolis and centripetal terms will be independent of the rotors' angular velocity.

To uniquely characterize the manipulator configuration, we choose the generalized coordinates $(\mathbf{q}\, \boldsymbol{\theta}) \in \mathbb{R}^{2N}$ being, respectively, the positions of the links and rotors reflected through the gear ratios; that is, the rotor positions are seen in the link space. Given assumptions (i)–(iii), the link and rotor dynamics become, respectively,

$$\mathbf{M}(\mathbf{q})\ddot{\mathbf{q}} + \mathbf{C}(\mathbf{q}, \dot{\mathbf{q}})\dot{\mathbf{q}} + \mathbf{g}(\mathbf{q}) = \boldsymbol{\tau}_J, \tag{1}$$

$$\mathbf{B}\,\ddot{\boldsymbol{\theta}} + \mathbf{f} + \boldsymbol{\tau}_J = \mathbf{K}_\tau\, \mathbf{i}, \tag{2}$$

where, in the link equation, $\mathbf{M}(\mathbf{q}) > 0 \in \mathbb{R}^{N \times N}$ is the symmetric inertia matrix, $\mathbf{C}(\mathbf{q}, \dot{\mathbf{q}}) \in \mathbb{R}^{N \times N}$ is the Coriolis and centripetal matrix, $\mathbf{g}(\mathbf{q}) \in \mathbb{R}^N$ is the gravity vector, and $\boldsymbol{\tau}_J \in \mathbb{R}^N$ is the vector of joint torques which couple the link and rotor subsystems. In the rotor equation, $\mathbf{B} > 0 \in \mathbb{R}^{N \times N}$ is the diagonal matrix of rotor inertias, $\mathbf{f} \in \mathbb{R}^N$ is friction acting on the rotor coordinate, $\mathbf{K}_\tau > 0 \in \mathbb{R}^{N \times N}$ is the diagonal matrix of torque constants, and $\mathbf{i} \in \mathbb{R}^N$ is the torque-generating (quadrature) current obtained from the phase currents via Park's Transformation. The drive-gain $\mathbf{K}_\tau$ has been calibrated *a* priori with special tests; see, for example, [21].

The dynamic model of the N link robot manipulator is obtained in closed form using the Denavit-Hartenberg (DH) convention [22] with coordinate systems placed as illustrated in Figure 3 to represent the UR5e manipulator and with the parameters in Table 1 and the Recursive Newton–Euler Algorithm (RNEA) [22]. In the RNEA, the position vector ${}^i\mathbf{P}_{i+1} = [a_{i-1} \;\; -d_i \sin(\alpha_{i-1}) \;\; d_i \cos(\alpha_{i-1})]^T$ and the rotation matrix

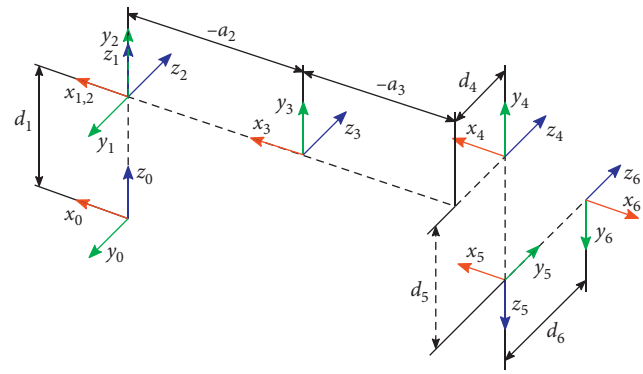

Figure 3: Coordinate systems used for describing the kinematics of the UR5e robot using the Denavit–Hartenberg convention.

Table 1: Denavit–Hartenberg parameters of the UR5e robot.

i	a_i	α_i	d_i	q_i
1	0	$\pi/2$	d_1	q_1
2	a_2	0	0	q_2
3	a_3	0	0	q_3
4	0	$\pi/2$	d_4	q_4
5	0	$-\pi/2$	d_5	q_5
6	0	0	d_6	q_6

$$
{}^{i+1}_{i}\mathbf{R} = \begin{bmatrix} \cos(q_i) & -\sin(q_i) & 0 \\ \sin(q_i)\cos(\alpha_{i-1}) & \cos(q_i)\cos(\alpha_{i-1}) & -\sin(\alpha_{i-1}) \\ \sin(q_i)\sin(\alpha_{i-1}) & \cos(q_i)\sin(\alpha_{i-1}) & \cos(\alpha_{i-1}) \end{bmatrix}. \tag{3}
$$

To allow a parametrization of the dynamics which is linear in the inertial parameters, the inertia tensor for each link is defined relative to the center of rotation (CoR). The RNE algorithm needs the inertia tensor defined relative to the center of mass (CoM), so the parallel axis theorem (Steiner's law) is used for translation; that is,

$$
\mathbf{I}_{\mathrm{CoM},i} = \mathbf{I}_{\mathrm{CoR},i} - m_i\left(\left(\mathbf{P}_{C,i}^T\mathbf{P}_{C,i}\right)\mathbf{E}_3 - \mathbf{P}_{C,i}\mathbf{P}_{C,i}^T\right), \tag{4}
$$

with $\mathbf{E}_3$ being the 3×3 identity matrix, and the vector of center of mass positions $\mathbf{P}_{C,i} = \begin{bmatrix} P_{C,i,x} & P_{C,i,y} & P_{C,i,z} \end{bmatrix}^T$, m_i is the mass of link i, and the symmetric inertia tensor is

$$
\mathbf{I}_{\mathrm{CoR},i} = \begin{bmatrix} \mathrm{XX}_i & \mathrm{XY}_i & \mathrm{XZ}_i \\ \mathrm{XY}_i & \mathrm{YY}_i & \mathrm{YZ}_i \\ \mathrm{XZ}_i & \mathrm{YZ}_i & \mathrm{ZZ}_i \end{bmatrix}. \tag{5}
$$

3. Dynamics Parametrization

The expressions for the torques obtained from the RNE algorithm can be expressed linearly in the inertial parameters:

$$
\boldsymbol{\tau}_J = \mathbf{Y}(\mathbf{q}, \dot{\mathbf{q}}, \ddot{\mathbf{q}})\boldsymbol{\gamma}, \tag{6}
$$

where the inertial parameters are

$$
\begin{aligned}
\boldsymbol{\gamma} &= \left[\boldsymbol{\gamma}_1^T \cdots \boldsymbol{\gamma}_i^T \cdots \boldsymbol{\gamma}_N^T\right]^T, \\
\boldsymbol{\gamma}_i &= \left[\mathrm{XX}_i\ \mathrm{XY}_i\ \mathrm{XZ}_i\ \mathrm{YY}_i\ \mathrm{YZ}_i\ \mathrm{ZZ}_i\ m\mathrm{X}_i\ m\mathrm{Y}_i\ m\mathrm{Z}_i\ m_i\right]^T.
\end{aligned} \tag{7}
$$

For a specific robot manipulator, not all 10 N inertial parameters can be identified. Not all the inertial parameters have an effect on the dynamic model, while others have an effect only in linear combinations. The inertial parameters of a robot can therefore be classified into three groups: fully identifiable, identifiable in linear combinations only, and unidentifiable. This is due to the kinematic arrangement of the joints as well as the orientation of the manipulator's base with respect to gravity. Table 2 shows the 49 inertial parameters that appear in the mathematical model.

For the estimation problem to have a unique solution, the parameters must be linearly independent. The set of linearly independent parameters is called *base parameters*. The number of base parameters b_m is [23]

$$
b_m \leq 7n_r + 4n_p - 3 - \overline{\sigma}_1 - 2n_{g0}, \tag{8}
$$

where n_r is the number of revolute joints, n_p is the number of prismatic joints, and $\overline{\sigma}_1 = 1$ if joint 1 is revolute; otherwise $\overline{\sigma}_1 = 0$; and $n_{g0} = 1$ if the rotation axis of joint 1 is parallel to the direction of the gravitational acceleration; otherwise $n_{g0} = 0$. For a robot manipulator with the kinematic arrangement in Table 1 and the base joint oriented with its rotation axis parallel to the direction of the gravitational acceleration, the number of base parameters $b_m = 36$. Therefore, a number of inertial parameters are grouped into a fewer number of equivalent parameters using the regrouping relations [24]:

Table 2: The 49 inertial parameters that appear in the dynamic model of the UR5e manipulator when mounted such that the rotation axis of the base joint is oriented parallel to the gravitational acceleration.

i	XX_i	XY_i	XZ_i	YY_i	YZ_i	ZZ_i	$m\mathrm{X}_i$	$m\mathrm{Y}_i$	$m\mathrm{Z}_i$	m_i
1	–	–	–	–	–	ZZ_1	–	–	–	–
2	XX_2	XY_2	XZ_2	YY_2	YZ_2	ZZ_2	$m_2P_{C,2,x}$	$m_2P_{C,2,y}$	–	–
3	XX_3	XY_3	XZ_3	YY_3	YZ_3	ZZ_3	$m_3P_{C,3,x}$	$m_3P_{C,3,y}$	$m_3P_{C,3,z}$	m_3
4	XX_4	XY_4	XZ_4	YY_4	YZ_4	ZZ_4	$m_4P_{C,4,x}$	$m_4P_{C,4,y}$	$m_4P_{C,4,z}$	m_4
5	XX_5	XY_5	XZ_5	YY_5	YZ_5	ZZ_5	$m_5P_{C,5,x}$	$m_5P_{C,5,y}$	$m_5P_{C,5,z}$	m_5
6	XX_6	XY_6	XZ_6	YY_6	YZ_6	ZZ_6	$m_6P_{C,6,x}$	$m_6P_{C,6,y}$	$m_6P_{C,6,z}$	m_6

$$
\begin{aligned}
\mathrm{XXR}_i &= \mathrm{XX}_i - \mathrm{YY}_i,\\
\mathrm{XXR}_{i-1} &= \mathrm{XX}_{i-1} + \mathrm{YY}_i + 2d_i m\mathrm{Z}_i + d_i^2 m_i,\\
\mathrm{XYR}_{i-1} &= \mathrm{XY}_{i-1} + a_{i-1}\sin(\alpha_i)m\mathrm{Z}_i + a_{i-1}d_i\sin(\alpha_i)m_i,\\
\mathrm{XZR}_{i-1} &= \mathrm{XZ}_{i-1} - a_{i-1}\cos(\alpha_i)m\mathrm{Z}_i - a_{i-1}d_i\cos(\alpha_i)m_i,\\
\mathrm{YYR}_{i-1} &= \mathrm{YY}_{i-1} + \cos^2(\alpha_i)\mathrm{YY}_i + 2d_i\cos^2(\alpha_i)m\mathrm{Z}_i + \left(\alpha_{i-1}^2 + d_i^2\cos^2(\alpha_i)\right)m_i,\\
\mathrm{YZR}_{i-1} &= \mathrm{YZ}_{i-1} + \cos(\alpha_i)\sin(\alpha_i)\mathrm{YY}_i + 2d_i\cos(\alpha_i)\sin(\alpha_i)m\mathrm{Z}_i + d_i^2\cos(\alpha_i)\sin(\alpha_i)m_i,\\
\mathrm{ZZR}_{i-1} &= \mathrm{ZZ}_{i-1} + \sin^2(\alpha_i)\mathrm{YY}_i + 2d_i\sin^2(\alpha_i)m\mathrm{Z}_i + \left(a_{i-1}^2 + d_i^2\sin^2(\alpha_i)\right)m_i,\\
m\mathrm{XR}_{i-1} &= m\mathrm{X}_{i-1} + a_{i-1}m_i,\\
m\mathrm{YR}_{i-1} &= m\mathrm{Y}_{i-1} - \sin(\alpha_i)m\mathrm{Z}_i - d_i\sin(\alpha_i)m_i,\\
m\mathrm{ZR}_{i-1} &= m\mathrm{Z}_{i-1} + \cos(\alpha_i)m\mathrm{Z}_i + d_i\cos(\alpha_i)m_i,\\
m\mathrm{R}_{i-1} &= m_{i-1} + m_i.
\end{aligned}
\tag{9}
$$

This results in the set of base parameters in Table 3.

The joint torque is expressed as

$$\boldsymbol{\tau}_J = \mathbf{Y}_b(\mathbf{q}, \dot{\mathbf{q}}, \ddot{\mathbf{q}})\boldsymbol{\gamma}_b, \tag{10}$$

with the vector of base parameters

$$\boldsymbol{\gamma}_b = \left[\mathrm{ZZR}_1\ \mathrm{XXR}_2\ \cdots\ m\mathrm{Y}_6\right]^T \in \mathbb{R}^{b_m}. \tag{11}$$

3.1. Including the Rotor Dynamics. Combining (2) and (10) yields

$$\mathbf{K}_\tau\,\mathbf{i} - \mathbf{B}\,\ddot{\boldsymbol{\theta}} - \mathbf{f} = \mathbf{Y}_b(\mathbf{q}, \dot{\mathbf{q}}, \ddot{\mathbf{q}})\boldsymbol{\gamma}_b. \tag{12}$$

Friction torques are considered as a sum of estimates and error terms. From experience and empirical observations, the error $\widetilde{\mathbf{f}} \triangleq \mathbf{f} - \widehat{\mathbf{f}}$ is assumed to contain Coulomb and viscous friction contributions; that is, $\widetilde{\mathbf{f}} = \widetilde{\mathbf{F}}_C\,\mathrm{sgn}(\dot{\boldsymbol{\theta}}) + \widetilde{\mathbf{F}}_V\,\dot{\boldsymbol{\theta}}$. The nonlinear estimates, as presented in [19], describe the friction torques in terms of the angular velocities, load torques, and temperatures. Rotor inertias $\mathbf{B}$ are considered to be known; however, they could be easily estimated by augmenting the regressor with the angular acceleration of the rotors. The system formulated in terms of base parameters and augmented with the rotor dynamics and friction discrepancy is

$$\boldsymbol{\tau}_J = \mathbf{Y}_B(\mathbf{q}, \dot{\mathbf{q}}, \ddot{\mathbf{q}})\boldsymbol{\gamma}_B + \boldsymbol{\rho}, \tag{13}$$

$$\boldsymbol{\tau}_J = \mathbf{K}_\tau\mathbf{i} - \mathbf{B}\,\ddot{\boldsymbol{\theta}} - \widehat{\mathbf{f}}, \tag{14}$$

$$\mathbf{Y}_B(\mathbf{q}, \dot{\mathbf{q}}, \ddot{\mathbf{q}}) = \left[\mathbf{Y}_b(\mathbf{q}, \dot{\mathbf{q}}, \ddot{\mathbf{q}})\ \ \mathrm{diag}(\mathbf{sgn}(\dot{\boldsymbol{\theta}}))\ \ \mathrm{diag}(\dot{\boldsymbol{\theta}})\right], \tag{15}$$

$$\boldsymbol{\gamma}_B = \left[\boldsymbol{\gamma}_b^T\ \ \mathrm{diag}^{-1}\left(\widetilde{\mathbf{F}}_\mathbf{C}\right)^T\mathrm{diag}^{-1}\left(\widetilde{\mathbf{F}}_\mathbf{V}\right)^T\right]^T, \tag{16}$$

where the noise $\boldsymbol{\rho}$ due to model errors and measurement noise is assumed to have zero mean, be serially uncorrelated, and be heteroskedastic, that is, having a diagonal covariance matrix.

4. Identification

This section presents the experimental setup, identification procedure, and results. The experiment is carried out using the setup shown in Figure 4. The system consists of the *UR5e* collaborative robot manipulator, Teach Pendant, Control Box, and PC. The estimation trajectory is generated using the Teach Pendant and is sent to the Control Box. The Control Box generates torque commands and sends them to the UR5e, and the measurements of actual values ($\mathbf{q}$, $\boldsymbol{\theta}$, and $\mathbf{i}$) are sent back from the UR5e to the Control Box. All the data are then logged by the PC.

The identification procedure is illustrated schematically in Figure 5.

Table 3: The 36 base parameters for the UR5e manipulator when mounted such that the rotation axis of the base joint is oriented parallel to the gravitational acceleration.

i	XX_i	XY_i	XZ_i	YZ_i	ZZ_i	mX_i	mY_i
1	–	–	–	–	ZZR_1	–	–
2	XXR_2	XY_2	XZR_2	YZ_2	ZZR_2	mXR_2	mY_2
3	XXR_3	XY_3	XZ_3	YZ_3	ZZR_3	mXR_3	mY_3
4	XXR_4	XY_4	XZ_4	YZ_4	ZZR_4	mX_4	mYR_4
5	XXR_5	XY_5	XZ_5	YZ_5	ZZR_5	mX_5	mYR_5
6	XXR_6	XY_6	XZ_6	YZ_6	ZZ_6	mX_6	mY_6

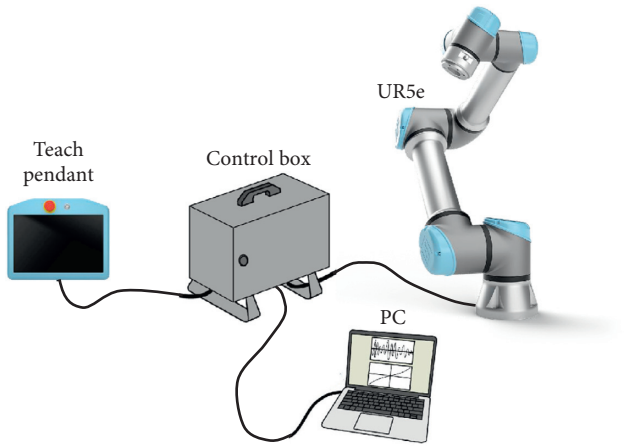

Figure 4: Experimental setup used for the dynamics identification.

Data is sampled at times $t(k) = kT_S, k = 1, 2, \ldots, M$, where $T_S = 1$ ms is the sampling period, and the sampling frequency $f_S = 1$ kHz.

4.1. Joint Position, Velocity, and Acceleration Estimation. The measured trajectory data $\mathbf{q}$ and $\boldsymbol{\theta}$ are filtered by a 4^{th}-order Butterworth filter in both the forward and reverse directions to eliminate lag of the filtered trajectories $\widehat{\mathbf{q}}$ and $\widehat{\boldsymbol{\theta}}$. To keep the useful signal of the robot dynamics in the filter bandwidth, the cutoff frequency of the filter is chosen to be 5 times the frequency of the robot dynamics; that is, $5f_{\text{dyn}} = 50$ Hz. Angular velocities and accelerations $\dot{\widehat{\mathbf{q}}}$, $\ddot{\widehat{\mathbf{q}}}$, $\dot{\widehat{\boldsymbol{\theta}}}$, and $\ddot{\widehat{\boldsymbol{\theta}}}$, respectively, are obtained through a central difference procedure. The combination of the two-pass Butterworth filter and central difference is referred to as the band-pass filtering process.

4.2. Parallel Filtering and Downsampling. The sampling frequency is much higher than the frequencies of interest in the dynamics, so to reduce the required computational resources the data is parallel-filtered and then decimated/downsampled. Firstly, the samples $k = 1, \ldots, M$ are ordered in the measurement vector $\mathbf{y}_i$ and observation matrix $\mathbf{W}_i$ for each joint $i = 1, \ldots, N$ individually; that is,

$$\begin{aligned} \overline{y}_i &= \left[\tau_{J,i,1} \cdots \tau_{J,i,k} \cdots \tau_{J,i,M}\right]^T, \\ \overline{\mathbf{W}}_i &= \left[\mathbf{W}_{i,1}^T \cdots \mathbf{W}_{i,k}^T \cdots \mathbf{W}_{i,M}^T\right]^T, \\ \mathbf{W}_{i,k} &= \mathbf{Y}_{B,i}\left(\widehat{\mathbf{q}}_k, \dot{\widehat{\mathbf{q}}}_k, \ddot{\widehat{\mathbf{q}}}_k\right), \end{aligned} \tag{17}$$

with $\mathbf{Y}_{B,i}(\widehat{\mathbf{q}}_k, \dot{\widehat{\mathbf{q}}}_k, \ddot{\widehat{\mathbf{q}}}_k)$ being the i^{th} row of the regressor evaluated in the k^{th} sample of the filtered trajectory. The parallel filtering of the measurement vector and observation matrix for each joint is conducted by passing the signals through a 4^{th}-order Butterworth filter in both the forward and reverse directions having a cut-off frequency of $2f_{\text{dyn}} = 20$ Hz. The downsampling factor is $0.8f_S/(4f_{\text{dyn}}) = 20$ [10]; that is, every 20^{th} sample is used for parameter estimation. The filtering and downsampling of $\overline{\mathbf{y}}_i$ and $\overline{\mathbf{W}}_i$ produce estimates $\mathbf{y}_i$ and $\mathbf{W}_i$, respectively.

4.3. Torque Computation. The filtered and downsampled data are ordered joint-wise in the measurement vector and observation matrix as

$$\begin{aligned} \mathbf{y} &= \left[\mathbf{y}_1^T \cdots \mathbf{y}_i^T \cdots \mathbf{y}_N^T\right]^T \in \mathbb{R}^{N \cdot M}, \\ \mathbf{W} &= \left[\mathbf{W}_1^T \cdots \mathbf{W}_i^T \cdots \mathbf{W}_N^T\right]^T \in \mathbb{R}^{N \cdot M \times b_m}. \end{aligned} \tag{18}$$

The base parameters are estimated by solving the WLS problem:

$$\begin{aligned} \widehat{\boldsymbol{\gamma}}_B &= \arg\min_{\boldsymbol{\gamma}_B} \left\|\mathbf{W}^T\mathbf{G}\left(\mathbf{y} - \mathbf{W}\boldsymbol{\gamma}_B\right)\right\|^2 \\ &= \left(\mathbf{W}^T\mathbf{G}\mathbf{W}\right)^{-1}\mathbf{W}^T\mathbf{G}\mathbf{y}, \end{aligned} \tag{19}$$

where each weight in $\mathbf{G}$ is equal to the reciprocal of the estimated standard deviation of the error.

$$\begin{aligned} \mathbf{G} &= \operatorname{diag}(\mathbf{S}), \\ \mathbf{S} &= \left[\mathbf{S}_1 \ \ldots \ \mathbf{S}_i \ \ldots \ \mathbf{S}_N\right], \\ \mathbf{S}_i &= \left[\frac{1}{\widehat{\sigma}_{i,1}} \ldots \frac{1}{\widehat{\sigma}_{i,j}} \ldots \frac{1}{\widehat{\sigma}_{i,b_{m,i}}}\right], \quad j = 1, \ldots, b_{m,i}, \\ \widehat{\sigma}_{i,j}^2 &= \frac{\left\|\boldsymbol{\tau}_i - \mathbf{Y}_{B,i}\widehat{\boldsymbol{\gamma}}_{B,i}\right\|^2}{M - b_{m,i}}, \end{aligned} \tag{20}$$

with $b_{m,i}$ being the number of base parameters related to link i. Such weighting operation normalizes the error terms in (13).

4.4. Trajectory. The trajectory used for parameter estimation should allow complete identification of the system; that is, for positive constants α and β, it should satisfy some persistently exciting condition:

$$\beta\mathbf{E} \geq \int_0^T \mathbf{W}^T\mathbf{W}\mathrm{d}t \geq \alpha\mathbf{E}, \tag{21}$$

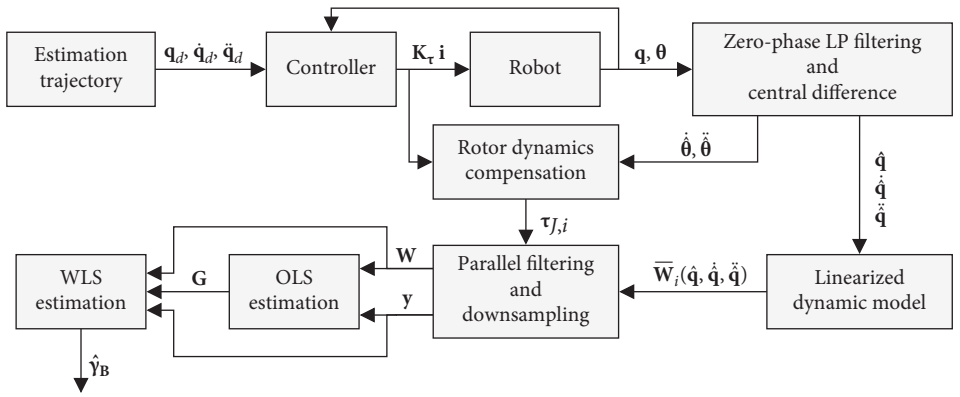

Figure 5: Schematic representation of the Inverse Dynamics Identification Model with Weighted Least Squares (IDIM-WLS) estimation and *rotor dynamics compensation* procedure. The estimation trajectory sends desired angular positions $\mathbf{q}_d, \dot{\mathbf{q}}_d, \ddot{\mathbf{q}}_d$ to the *controller*, which generates torque commands $\mathbf{K}_t\mathbf{i}$ to the robot. The angular positions of the links and rotors, $\mathbf{q}$ and $\boldsymbol{\theta}$, respectively, are measured and then filtered to generate smoothed estimates $\hat{\mathbf{q}}$ and time-derivatives $\dot{\hat{\mathbf{q}}}$, $\ddot{\hat{\mathbf{q}}}$, $\dot{\hat{\boldsymbol{\theta}}}$, and $\ddot{\hat{\boldsymbol{\theta}}}$. The rotor quantities are passed to the *Rotor dynamics compensation*, and the link quantities are passed to the *Linearized dynamic model*. The *Rotor dynamics compensation* augments the measured current with the rotor dynamics based on (15) to estimate joint torques $\boldsymbol{\tau}_J$. The *Linearized dynamic model* generates regressors $\overline{\mathbf{W}}_i$ for each joint i. The joint torque estimates and regressors are filtered and downsampled to generate, respectively, the measurement vector $\mathbf{y}$ and observation matrix $\mathbf{W}$. The measurement vector and observation matrix are passed to the *OLS Estimation* and *WLS estimation* procedures. The OLS procedure produces the weighting matrix $\mathbf{G}$ used in the WLS procedure. Finally, the *WLS estimation* provides the dynamic parameters estimates $\hat{\boldsymbol{\gamma}}_B$.

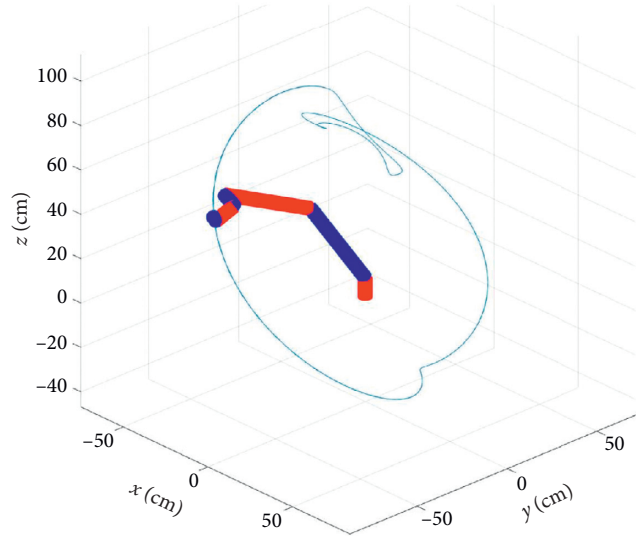

Figure 6: Trajectory used for the parameter estimation yielding a low condition number of the regressor matrix $\text{cond}(\mathbf{W}) = 66$.

where α is the degree of excitation and β/α is the condition number of $\mathbf{W}^T\mathbf{W}$. The trajectory in Figure 6 is used for yielding a condition number for the regressor $\text{cond}(\mathbf{W}) = 66$. The trajectory is 31 seconds long; hence, with a sampling frequency of 1000 Hz and a downsampling factor of 20, the total number of samples is 1550. Another approach to the trajectory design is to optimize the condition number of the regressor with respect to the trajectory subject to kinematic and dynamic constraints, for example, position, velocity, acceleration, and current.

4.5. Model Quality Metric. The model quality is evaluated by the sum of each joint's mean squared error normalized by its average torque magnitude; that is,

$$\text{NMSE} = \sum_{j=1}^{N}\sum_{k=1}^{M}\frac{\left(\tau_{J,i,k} - \hat{\tau}_{J,i,k}\right)^2}{\left|\tau_{J,i,k}\right|}. \tag{22}$$

4.6. Results. Values of the identified base parameters are shown in Table 4. The effectiveness of the method is demonstrated by considering the accuracy of the dynamic model with the optimized parameters compared to our baseline, a model with parameters obtained through CAD software. The model accuracy improves 81.4% from a NMSE of 506.8 Nm to that of 94.5 Nm.

The parameters are generally well estimated with small relative standard deviations, which demonstrates the

Table 4: Estimated values and relative standard deviation of the 36 base parameters obtained by solving the WLS problem with rotor dynamics compensation.

Base param.	Value	$\%\sigma_{\widehat{\gamma_B}}$
ZZR_1	2.1981	0.099
XXR_2	−1.6552	0.130
XY_2	−0.0405	1.975
XZR_2	0.3734	0.210
YZ_2	0.1278	1.367
ZZR_2	−4.1774	0.198
mXR_2	−0.0132	0.001
mY_2	−0.7336	0.141
XXR_3	−0.1563	0.166
XY_3	0.1302	0.225
XZ_3	−0.1714	0.249
YZ_3	0.0212	0.433
ZZR_3	−1.8774	2.908
mXR_3	0.0428	0.001
mY_3	−0.0428	0.030
XXR_4	−0.0454	0.609
XY_4	0.0144	0.422
XZ_4	0.0166	0.767
YZ_4	0.0005	18.894
ZZR_4	−0.0005	20.082
mX_4	−0.0112	0.043
mYR_4	−0.1866	0.001
XXR_5	0.0239	0.450
XY_5	−0.0391	0.055
XZ_5	0.0194	0.080
YZ_5	0.0065	0.286
ZZR_5	0.0315	0.076
mX_5	−0.0013	0.137
mYR_5	0.0442	0.005
XXR_6	0.0187	0.132
XY_6	0.0059	0.107
XZ_6	0.0187	0.054
YZ_6	−0.0002	3.825
ZZ_6	0.0209	0.157
mX_6	0.0036	0.040
mY_6	−0.0043	0.041

effectiveness of the identification procedure. The values of parameters YZ_4 and ZZR_4 are, however, subject to relative standard deviations of 19% and 20%, respectively. This is an indication of either (1) suboptimality of the chosen trajectory or (2) the parameter being of no big value to the torque computation. YZ_4 is a product moment of inertia (off-diagonal element in the inertia tensor) and is therefore likely to be less important in the dynamics. ZZR_4 is a mass moment of inertia (diagonal element in the inertia tensor) and the reduced accuracy in its estimation is likely due to insufficient excitation by the chosen trajectory.

5. Validation

The purpose of the dynamic model calibration is to improve the torque estimation accuracy for arbitrary trajectories. Thus, we evaluate the accuracy of our calibrated model on three trajectories different from the one used for parameter estimation. The measured joint torques are compared to the torques output by the calibrated dynamic model as well as relative to our CAD model baseline. Improvements in NMSE and improvements relative to our baseline are shown in Table 5. The results show a relative improvement of the calibrated dynamic model compared to the dynamic model

Table 5: Normalized Mean Squared Error (NMSE) of the dynamic models; CAD model with parameters obtained from a CAD model of the robot and calibrated with parameters estimated through the WLS procedure with rotor dynamics compensation. Improvements in NMSE and relative to CAD model for three different trajectories.

Traj.	NMSE CAD model	NMSE calibrated	Relative improvement (%)
1	325.9	233.0	28.5
2	1245.7	1040.4	16.5
3	334.0	250.9	24.9

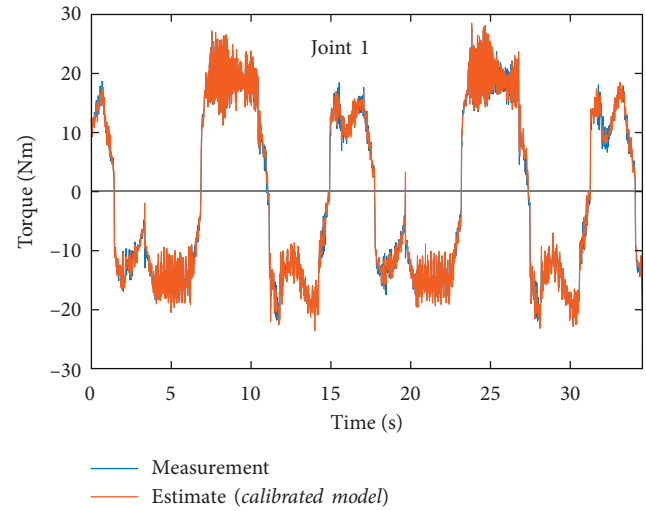

Figure 7: Results of measurement and estimate using the calibrated parameters on the validation trajectory.

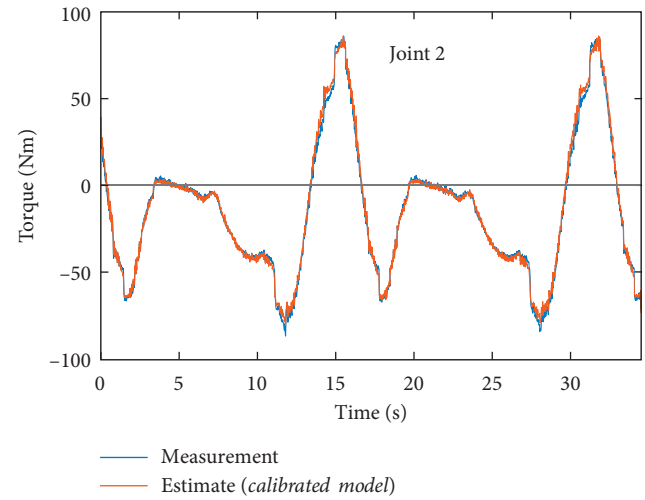

Figure 8: Results of measurement and estimate for joint no. 2 with the calibrated parameters.

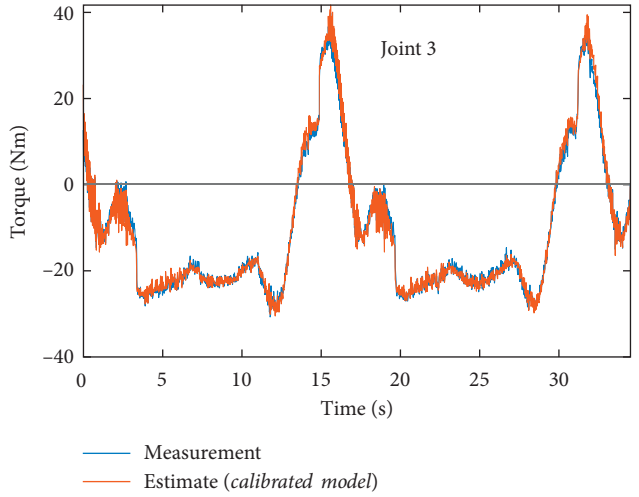

Figure 9: Results of measurement and estimate for joint no. 3 with the calibrated parameters.

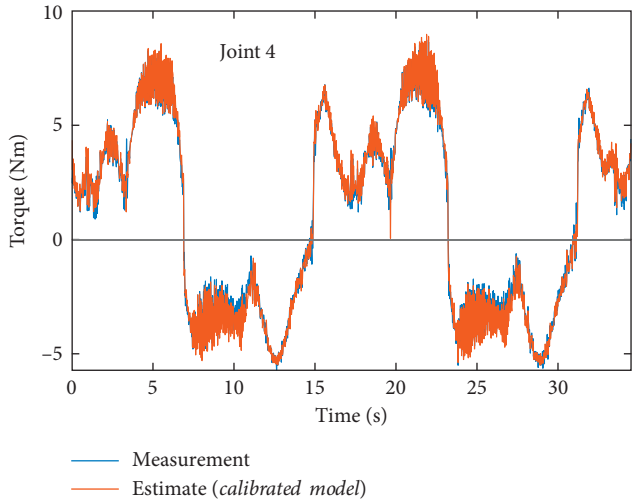

Figure 10: Results of measurement and estimate for joint no. 4 with the calibrated parameters.

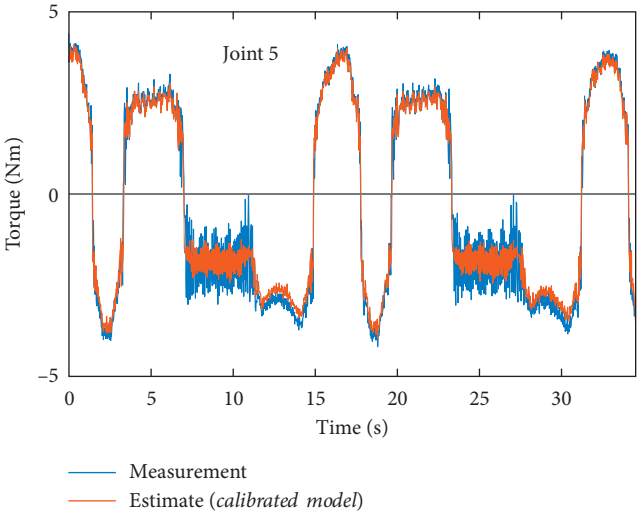

Figure 11: Results of measurement and estimate for joint no. 5 with the calibrated parameters.

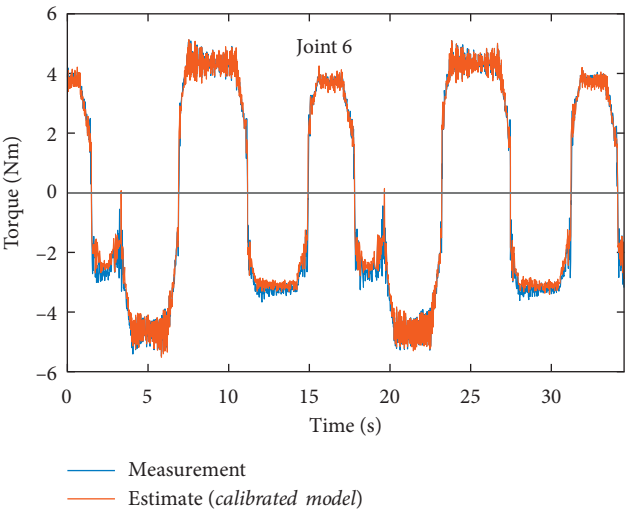

Figure 12: Results of measurement and estimate for joint no. 6 with the calibrated parameters.

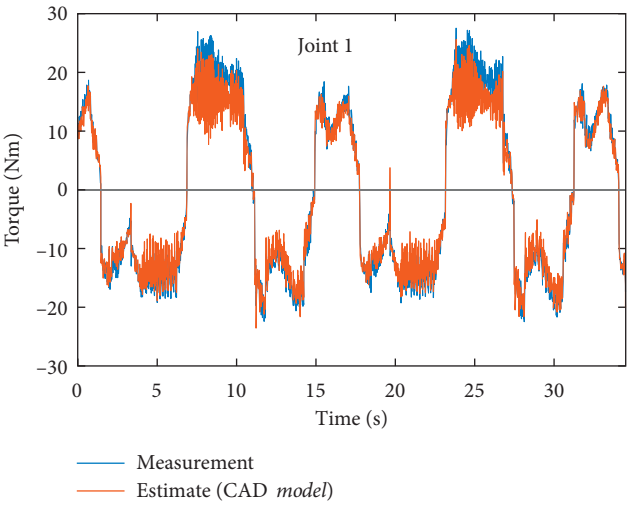

Figure 13: Results of measurement and estimate for joint no. 1 with the CAD model parameters.

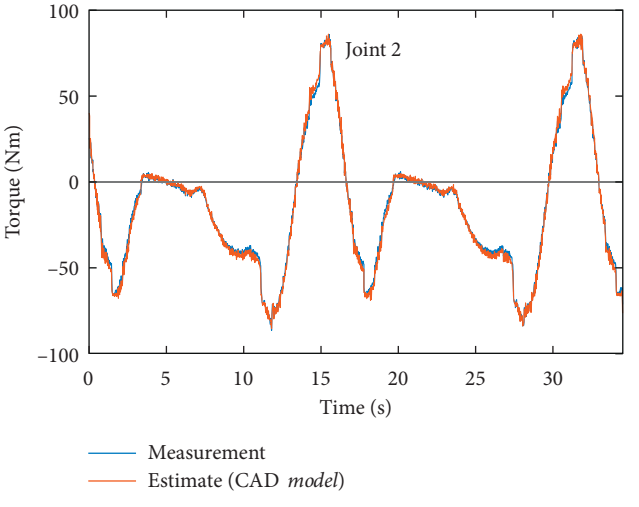

Figure 14: Results of measurement and estimate for joint no. 2 with the CAD model parameters.

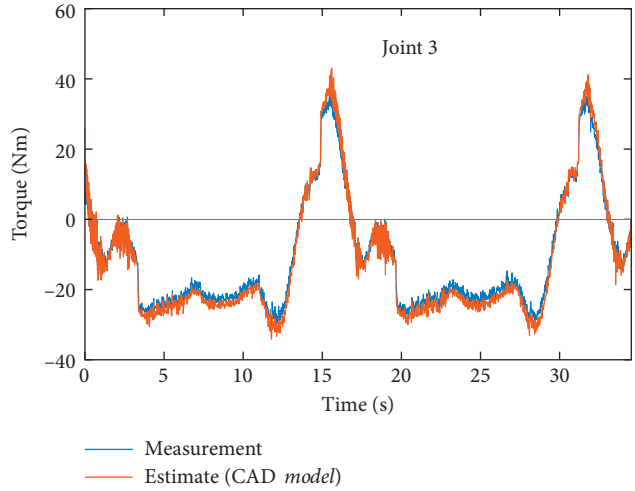

Figure 15: Results of measurement and estimate for joint no. 3 with the CAD model parameters.

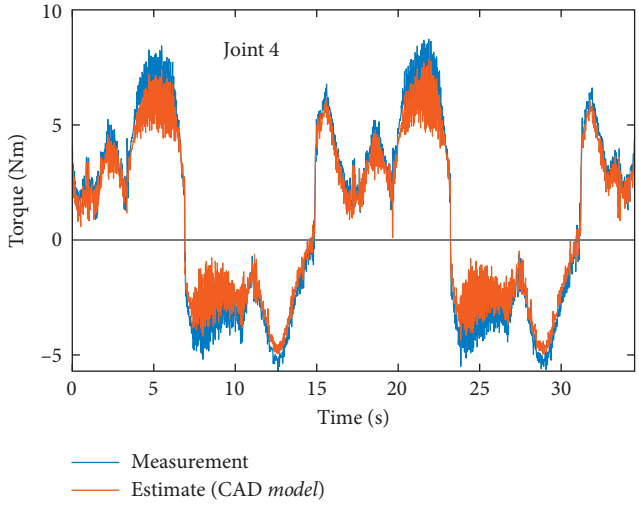

Figure 16: Results of measurement and estimate for joint no. 4 with the CAD model parameters.

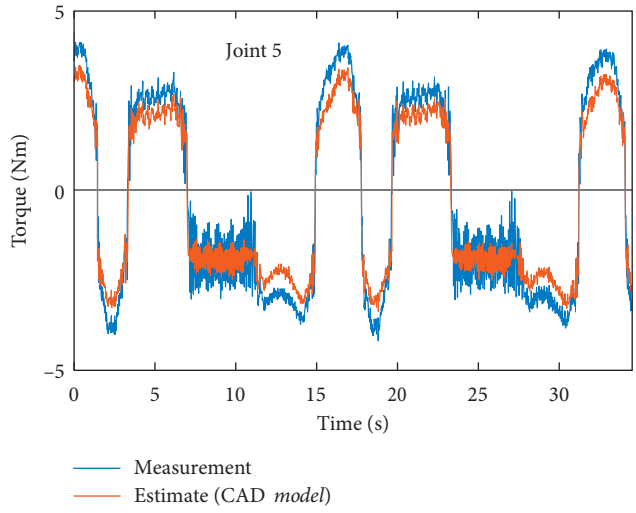

Figure 17: Results of measurement and estimate for joint no. 5 with the CAD model parameters.

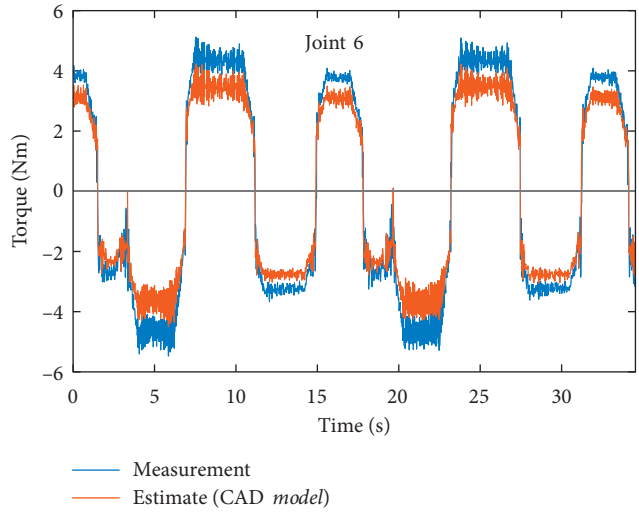

Figure 18: Results of measurement and estimate for joint no. 6 with the CAD model parameters.

with CAD parameters of 16.5%–28.5% depending on the trajectory. Time-series torque data for each of the joints of the UR5e dynamic model with calibrated parameters are shown in Figures 7–12 for trajectory no. 1. Time-series torque data for each of the joints of the *UR5e* dynamic model with CAD model parameters are shown in Figures 13–18 for trajectory no. 1. The reduction in torque prediction error (NMSE) of 16.5%–28.5% of the calibrated dynamic model compared to the dynamic model with CAD model parameters together with the time-series torque data in Figures 7–18 validates the effectiveness of the calibration procedure.

6. Conclusion

Collaborative industrial robots often utilize strain-wave type transmissions due to their desirable characteristics of high torque capacity and low weight. However, their inherent complex nonlinear behavior introduces significant errors and uncertainties in the robot dynamics calibration, resulting in decreased performance for motion and force control tasks and lead-through programming applications.

This paper presented a new method for the dynamics parametrization and calibration of collaborative industrial robot manipulators. The method combines the IDIM-WLS method for rigid robot dynamics with complex nonlinear expressions for the rotor-side dynamics to obtain increased calibration accuracy. Two angular position measurements per robot joint are utilized, one at each side of the strain-wave transmission, to effectively compensate the rotor inertial torques and nonlinear dynamic friction that were identified in our previous works.

The effectiveness of the method was demonstrated by the application to the Universal Robots UR5e collaborative robot manipulator. The results were very accurate estimates of the dynamic parameters. Relative improvement of 16.5% to 28.5% compared to a CAD model baseline was experienced.

The distinguished contributions of this work can be summarized as follows: (1) a linear parametrization describing the dynamics of the UR5e collaborative robot manipulator has been developed, (2) the complex nonlinear dynamic friction characteristics and rotor inertia have been considered, (3) the minimal set of base parameters that describe the dynamic behavior of the UR5e robot has been accurately estimated, and (4) the performance of the calibrated dynamic model has been validated.

Our ongoing work that we are going to challenge consists of the following:

(1) The number of identifiable parameters can be increased by two (from 36 to 38) if the robot is mounted with the base joint axis of rotation not being parallel to the direction of the gravitational acceleration.

(2) The trajectory used for parameter optimization could possibly be optimized through the use of some optimization procedures. Such trajectory optimization procedures were discussed generally in [25] and applied in [26] on a KUKA 361 IR industrial robot.

(3) The optimization problem could be constrained to enforce the positive-definiteness of the inertia matrix using either Sylvester's theorem or Cholesky decomposition. This will ensure invertibility of the inertia matrix, which is useful for model-based control design. From Sylvester's theorem, it is possible to find conditions for the parameters [27], whereas, for Cholesky decomposition, a tolerance is defined and it takes the noise and measurement error into account [28].

Data Availability

Data are not available due to confidentiality and third-party rights.

Conflicts of Interest

The authors declare that they have no conflicts of interest reported in this paper.

Acknowledgments

This work was supported by the company Universal Robots A/S, Odense, Denmark, and Innovation Fund Denmark (Ref. no. 7038-00058B).

References

[1] C. Gaz and A. D. Luca, "Payload estimation based on identified coefficients of robot dynamics — with an application to collision detection," in *Proceedings of the 2017 IEEE/RSJ International Conference on Intelligent Robots and Systems (IROS)*, pp. 3033–3040, IEEE, Vancouver, Canada, September 2017.

[2] K. Kozlowski, *Modelling and Identification in Robotics*, Springer, London, UK, 1998.

[3] P. Poignet and M. Gautier, "Comparison of weighted least squares and extended Kalman filtering methods for dynamic identification of robots," in *Proceedings of the 2000 ICRA, IEEE International Conference on Robotics and Automation. Symposia Proceedings (Cat. No.00CH37065)*, April 2000.

[4] M. Gautier and P. Poignet, "Extended Kalman filtering and weighted least squares dynamic identification of robot," *Control Engineering Practice*, vol. 9, no. 12, pp. 1361–1372, 2001.

[5] G. Calafiore and M. Indri, "Robust calibration and control of robotic manipulators," in *Proceedings of the 2000 American Control Conference. ACC (IEEE Cat. No.00CH36334)*, June 2000.

[6] M. M. Olsen, J. Swevers, and W. Verdonck, "Maximum likelihood identification of a dynamic robot model: implementation issues," *The International Journal of Robotics Research*, vol. 21, no. 2, pp. 89–96, 2002.

[7] N. Ramdani and P. Poignet, "Robust dynamic experimental identification of robots with set membership uncertainty," *IEEE/ASME Transactions on Mechatronics*, vol. 10, no. 2, pp. 253–256, 2005.

[8] A. Janot, P. O. Vandanjon, and M. Gautier, "Using robust regressions and residual analysis to verify the reliability of LS estimation: application in robotics," in *Proceedings of the 2009 IEEE/RSJ International Conference on Intelligent Robots and Systems*, October 2009.

[9] A. Janot, P. O. Vandanjon, and M. Gautier, "Identification of 6 DOF rigid industrial robots with the instrumental variable method," *IFAC Proceedings*, vol. 45, no. 16, pp. 1659–1664, 2012.

[10] A. Janot, P.-O. Vandanjon, and M. Gautier, "A generic instrumental variable approach for industrial robot identification," *IEEE Transactions on Control Systems Technology*, vol. 22, no. 1, pp. 132–145, 2014.

[11] M. Gautier, A. Janot, and P.-O. Vandanjon, "A new closed-loop output error method for parameter identification of robot dynamics," *IEEE Transactions on Control Systems Technology*, vol. 21, no. 2, pp. 428–444, 2013.

[12] A. Janot, M. Gautier, A. Jubien, and P. O. Vandanjon, "Comparison between the CLOE method and the DIDIM method for robots identification," *IEEE Transactions on Control Systems Technology*, vol. 22, no. 5, pp. 1935–1941, 2014.

[13] K. K. Kumbla and M. Jamshidi, "Neural network based identification of robot dynamics used for neuro-fuzzy controller," in *Proceedings of the International Conference on Robotics and Automation*, April 1997.

[14] S. A. Kolyubin, A. S. Shiriaev, and A. Jubien, "Refining dynamics identification for Co-bots: case study on KUKA LWR4+ ∗ ∗this work was supported by the government of the Russian federation, GOSZADANIE no. 8.8885.2017/BP and grant 074-U01," *IFAC-PapersOnLine*, vol. 50, no. 1, pp. 14626–14631, 2017.

[15] Z. Shareef, P. Mohammadi, and J. Steil, "Improving the inverse dynamics model of the KUKA LWR IV+ using independent joint learning∗∗Z. Shareef received funding from the German federal ministry of education and research (BMBF) within the leading-edge cluster competition. P. Mohammadi received funding from the European community's horizon 2020 robotics program ICT-23-2014 under grant agreement 644727 - CogIMon," *IFAC-PapersOnLine*, vol. 49, no. 21, pp. 507–512, 2016.

[16] C. Gaz, M. Cognetti, A. Oliva, P. Robuffo Giordano, and A. De Luca, "Dynamic identification of the Franka Emika Panda robot with retrieval of feasible parameters using penalty-based optimization," *IEEE Robotics and Automation Letters*, vol. 4, no. 4, pp. 4147–4154, 2019.

[17] M. Taghbalout, J. F. Antoine, and G. Abba, "Experimental dynamic identification of a YuMi collaborative robot," *IFAC-PapersOnLine*, vol. 52, no. 13, pp. 1168–1173, 2019.

[18] E. Madsen, O. S. Rosenlund, D. Brandt, and X. Zhang, "Model-based on-line estimation of time-varying nonlinear joint stiffness on an e-series universal robots manipulator," in *Proceedings of the 2019 International Conference on Robotics and Automation (ICRA)*, May 2019.

[19] E. Madsen, O. S. Rosenlund, D. Brandt, and X. Zhang, "Comprehensive modeling and identification of nonlinear joint dynamics for collaborative industrial robot manipulators," *Control Engineering Practice*, vol. 101.

[20] M. W. Spong, "Modeling and control of elastic joint robots," *Journal of Dynamic Systems, Measurement, and Control*, vol. 109, no. 4, pp. 310–318, 1987.

[21] P. P. Restrepo and M. Gautier, "Calibration of drive chain of robot joints," in *Proceedings of the International Conference on Control Applications*, September 1995.

[22] J. J. Craig, *Introduction to Robotics*, Pearson Education Limited, London, UK, 2013.

[23] M. Gautier and W. Khalil, "Direct calculation of minimum set of inertial parameters of serial robots," *IEEE Transactions on Robotics and Automation*, vol. 6, no. 3, pp. 368–373, 1990.

[24] M. Gautier and W. Khalil, "A direct determination of minimum inertial parameters of robots," in *Proceedings of the 1988 IEEE International Conference on Robotics and Automation*, pp. 1682–1687, Philadelphia, PA, USA, 1988.

[25] B. Armstrong, "On finding 'exciting' trajectories for identification experiments involving systems with non-linear dynamics," in *Proceedings of the 1987 IEEE International Conference on Robotics and Automation*, March-April 1987.

[26] J. Swevers, C. Ganseman, D. B. Tukel, J. de Schutter, and H. Van Brussel, "Optimal robot excitation and identification,"

IEEE Transactions on Robotics and Automation, vol. 13, no. 5, pp. 730–740, 1997.

[27] K. Yoshida and W. Khalil, "Verification of the positive definiteness of the inertial matrix of manipulators using base inertial parameters," *The International Journal of Robotics Research*, vol. 19, no. 5, pp. 498–510, 2000.

[28] M. Gautier and G. Venture, "Identification of standard dynamic parameters of robots with positive definite inertia matrix," in *Proceedings of the 2013 IEEE/RSJ International Conference on Intelligent Robots and Systems*, November 2013.